Journal of The Electrochemical Society, **148** (2) C124-C130 (2001)
0013-4651/2001/148(2)/C124/7/$7.00 © The Electrochemical Society, Inc.

Localized Electrodeposition Using a Scanning Tunneling Microscope Tip as a Nanoelectrode

W. Schindler,[a,z] D. Hofmann, and J. Kirschner

Max-Planck-Institut für Mikrostrukturphysik, D-06120 Halle, Germany

The mechanism of localized electrodeposition on the nanometer scale is studied using the tip of an electrochemical scanning tunneling microscope as a ''nanoelectrode,'' which is retracted from the substrate (working electrode) during growth of the clusters. The system chosen exemplarily is Au(111)/Co^{2+}, which shows a relatively weak substrate/deposit interaction compared to the strong interaction characteristic of underpotential deposition systems. The width and height of the clusters, which can be grown with diameters even below 10 nm, are determined by the diameter of the tip apex, the distance between tip and substrate, the substrate potential, and by the amount of Co transferred to the substrate via the tip. The influence of these parameters on the cluster growth can be well understood assuming diffusion as the mechanism of Co transfer from the tip to the substrate. Field and charging effects of either tip or substrate can be excluded due to the large distance of approximately 20 nm between both electrodes.
 [DOI: 10.1149/1.1343107]

Manuscript submitted June 19, 2000; revised manuscript received September 26, 2000.

The preparation of structures with lateral dimensions on the nanometer-scale attracts an increasing interest, since it has been shown that the physical and chemical properties of such nanostructures can strongly deviate from the properties of the corresponding bulk material.[1-3] Thus, nanotechnology opens up the promising possibility for tailoring novel properties of materials by varying the lateral structure size, and for exploiting even quantum effects for novel applications, *e.g.*, quantum logic circuits.[4] An example is the single electron transistor which operates at room temperature if its lateral structure size is confined to below 20 nm. This has been realized recently by a special nano-oxidation process using the tip of an atomic force microscope.[5,6] Nanostructures are also of great interest in other fields like, *e.g.*, magnetism[7-10] or electrocatalysis.[11-13]

In view of studying the size-dependent properties of model nanostructures it would be desirable to generate these structures at precisely, preset substrate positions. At present, scanning-probe-based nanostructure techniques seem to be suitable to fabricate nanostructures with lateral sizes below 20 nm, which is currently hard to achieve with existing lithographic techniques. However, it is most important that the generation of nanostructures is not accompanied by unwanted irreversible modifications of either the substrate, the nanostructure, or the scanning probe. Otherwise, the physical and chemical properties of nanostructures may be expected to be determined by the particular defects rather than by their intrinsic structure, particularly surface structure which increasingly determines the properties of ever smaller structures.

So far, a variety of scanning-probe-based methods have been reported in the literature.[14] They are on the one hand based on the specific pregeneration of defects which act as nucleation centers,[15-17] or on the other hand correlated with parasitic effects like field effects which may result in unwanted modification of either the substrate surface or the probe surface.[18-20] The mechanisms of all techniques which are applied with the probe in tunneling distance to the substrate is not very clear at present, and has been shown to be a superposition of different electrochemical and field effects,[21,22] even if mechanical contact can be excluded at all. An exception from these methods is the so-called ''jump to contact'' method by Kolb and co-workers,[23-25] which is not affected by unwanted field effects, but rather based on a controlled approach of the scanning tunneling microscope (STM) tip against the substrate. However, this technique seems to be applicable only in systems with a strong substrate/deposit interaction, *i.e.*, underpotential deposition (UPD) systems.[26] Recently, we have developed a technique which allows the solely electrochemical growth of Co clusters with diameters as small as 15 nm, as measured by STM, at the solid/liquid interface.[27,28]

In this paper, we present a detailed study of the different parameters of this localized electrocrystallization mechanism, using the STM tip as a nanometer-sized electrochemical electrode (Fig. 1). In contrast to the various nanostructuring techniques applied with the tip in the tunneling mode, we avoid parasitic effects or defect generation in either the substrate surface or at the STM probe by a large distance between STM tip and substrate surface during cluster growth. This simplifies the interpretation of the results, and allows a detailed discussion of the influence of different parameters on scanning-probe-based nanoscale electrocrystallization.

Experimental

The experiments have been performed with the electrochemical version of the Nanoscope III scanning tunneling microscope (Digital Instruments), which has been modified to vary the tip potential E_{tip} by external voltages independently of the substrate potential E_{WE}. Cathodic and anodic tip charges were determined by integration of the tip current I_{tip}. During the whole deposition sequence I_{tip} was monitored by a digitizing oscilloscope. The maximum tip current was limited by the modified current-voltage converter of our STM to 520 nA. During cluster deposition the STM tip was withdrawn from the substrate surface by means of the STM scanner piezoelements, and the feedback loop was disabled. The deposition experiments were performed in a conventional four-electrode electrochemical STM cell providing an electrolyte volume of about 100 μL. All potentials were measured *vs.* a saturated calomel reference electrode (SCE) (B 3105, Schott) which has been connected to the cell by a glass capillary, and are quoted in this paper with respect to the standard hydrogen electrode. The counter electrode was made from polycrystalline Pt wire. STM tips were prepared from Au wires of 0.25 mm diam by electrochemical etching in a lamella of HCl (32%), and then manually coated with Apiezon wax. These tips have been found to be well suited as electrochemical nanoelectrodes showing an electrochemical background current in the double layer regime of the current-voltage characteristics of smaller than 100 pA (Fig. 2) due to the small unisolated tip area which is of the order of 10 μm^2, as measured by scanning electron microscopy (SEM). As substrates Au(111) single crystals were chosen showing atomically flat terraces of several hundreds of nanometers after several cycles of flame-annealing. The aqueous electrolyte was made from ultrapure water (Milli-Q plus, Millipore), suprapure grade Na_2SO_4 (0.25 M), and $CoSO_4$ (1 mM), and was deaerated by purified nitrogen (99.999%, 5 N) prior and during the experiments. No additional additives were used in order to avoid any influence on the mechanism of cluster formation. The STM images were recorded in the

[a] Present address: Institut für Hochfrequenztechnik und Quantenelektronik, Universität Karlsruhe (TH), D-76131 Karlsruhe, Germany.
[z] E-mail: werner.schindler@eltec.uni-karlsruhe.de

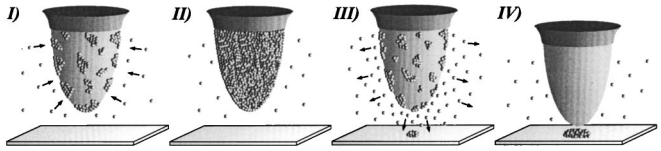

Figure 1. Schematic representation of the mechanism of Co cluster growth using the STM tip as a nanoelectrode. (I) Co deposition from the electrolyte onto the uncovered part of tip. (II) Co covered tip. (III) Co emitting tip during Co dissolution and localized cluster growth underneath the tip onto the substrate. (IV) Imaging of deposited clusters. The STM tip is retracted from the substrate during the whole deposition procedure.

constant current mode of the STM. The cluster width is specified as the full width at half maximum (fwhm) of the peak in the line profile through the center of the cluster.

Using the scanning probe tip as a nanoelectrode is a derivative of the concept of the scanning electrochemical microscope (SECM),[29,30] but it shows several important advantages. The electrochemical processes at the nanoelectrode are essentially reversible, and the nanoelectrode is electrochemically inert; its diameter is small compared to typical diameters of ultramicroelectrodes, or even capillaries; and it easily allows imaging *in situ* of the previously deposited structures by the scanning tunneling microscopy.

The Deposition Procedure

The deposition of Co clusters has been achieved by a two-step process using the STM tip as a nanoelectrode as shown schematically in Fig. 1. The distance of the STM tip from the substrate surface is between 10 and 30 nm during the deposition procedure. It is most important to avoid any mechanical contact of STM tip and subtrate. Thus, one can be sure not to induce irreversible modifications at either the substrate or the STM tip.

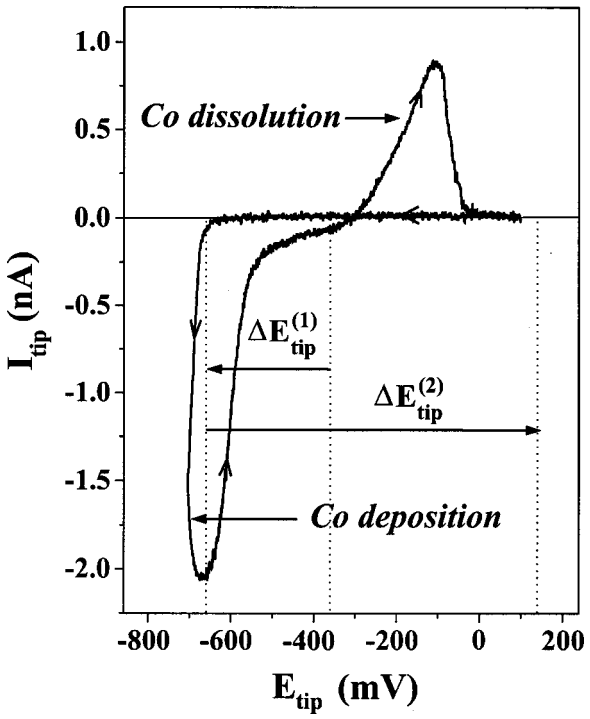

Figure 2. Cyclic voltammogram of the Co deposition onto the uncovered part of the Au STM tip. $\Delta E_{tip}^{(1)}$ denotes the potential jump in order to initiate Co deposition onto the tip, $\Delta E_{tip}^{(2)}$ the potential jump followed by an immediate Co dissolution from the tip. The arrows indicate the cycling direction of the potential with a sweep rate of 10 mV s^{-1}. (From Ref. 27.)

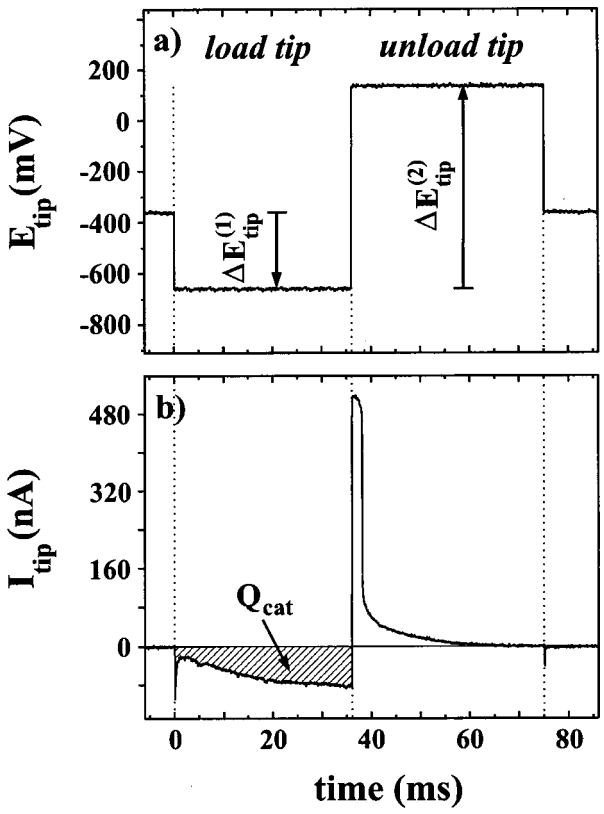

Figure 3. (a) Voltage and (b) current transients during deposition of Co onto the STM tip (load tip), and its subsequent dissolution from the STM tip (unload tip). Q_{cat} denotes the predeposited cathodic charge onto the STM tip. (From Ref. 28.)

During the first step of the deposition procedure Co is deposited from the electrolyte onto the uncoated part of the STM tip (Fig. 1, I) until the tip is covered with a preset amount of Co (Fig. 1, II). This is typically of the order of 10 to 20 monolayers of Co. The second step is the complete dissolution of Co from the STM tip (Fig. 1, III), which results in an increase of the Co^{2+} concentration around the STM tip, and particularly in the gap between the STM tip and the substrate. The increase of the Co^{2+} concentration around the STM tip results in an increase of the Co^{2+} concentration at the substrate surface opposite to the STM tip, which then causes an increase of the Nernst potential for Co^{2+} deposition within a certain area on the substrate underneath the STM tip. Co^{2+} will nucleate within this particular substrate area (Fig. 1, III, IV) at a properly adjusted substrate potential, positive to the bulk deposition equilibrium potential of the electrolyte, but smaller than the increased Nernst potential due to the Co dissolution from the STM tip.

The detailed potentials at the STM tip during deposition and dissolution of Co onto and from the tip, respectively, are shown in Fig. 2, the corresponding potential and current transients are plotted in Fig. 3. The deposition sequence starts with the uncovered tip at a tip potential of $E_{tip} = -360$ mV. Co deposition is achieved by a potential jump $\Delta E_{tip}^{(1)}$ into the cathodic potential regime. The measured current to the STM tip is diffusion limited during Co growth on the uncovered tip area. After deposition of a preadjusted amount of cathodic charge Q_{cat}, E_{tip} is switched by $\Delta E_{tip}^{(2)}$ into the anodic regime to dissolve Co from the STM tip. As is seen in Fig. 3, the measured Co^{2+} current during dissolution is limited to approximately 520 nA by the current-voltage converter of our STM, and lasts for about 2-3 ms depending on the preadjusted charge Q_{cat}.

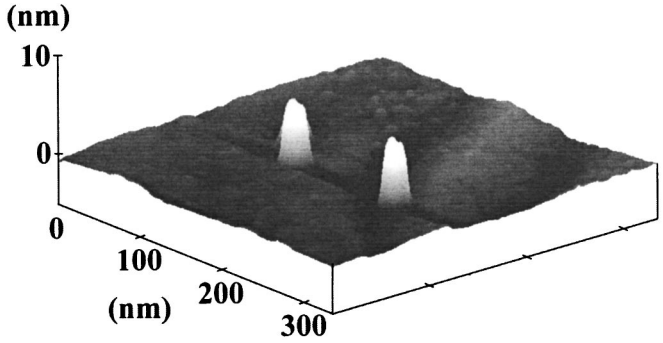

Figure 4. STM image of two Co clusters on Au(111) deposited by a twofold application of the deposition procedure with $Q_{cat} = 400$ pC. The fwhm of the clusters is 15 ± 1 nm, and the height 7.5 ± 0.5 nm as measured by STM. $E_{WE} = -530$ mV, $\Delta z = 15$ nm. The lower baselines of the STM scans across the clusters, compared to the substrate surface, are a scan artifact. (From Ref. 28.)

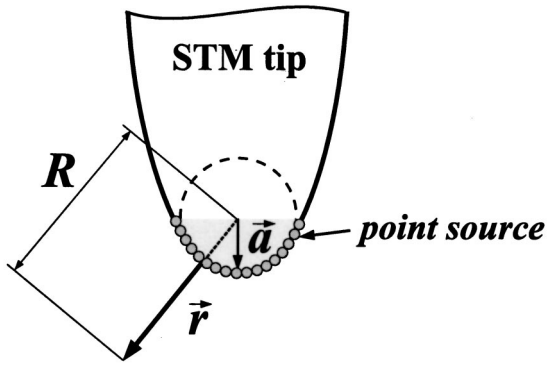

Figure 5. Schematic of the STM tip geometry assumed for the model calculation: The tip apex is modeled by a hemisphere of radius $\vec{a}$. The diffusion profile is calculated by integration of point sources across the surface of the hemisphere as indicated in the graph.

The procedure is reversible, since the Co film covering the STM tip is completely dissolved, except for unknown submonolayer alloying phenomena at the Au STM tip, and can hence be repeated many times without alteration of the shape of the Au STM tip. This feature also allows a subsequent *in situ* imaging of the deposited structures. Such an imaging would not be possible in the case of a pure Co nanoelectrode, because the Co dissolution would change the shape of this electrode.

Figure 4 shows two Co clusters on a Au(111) terrace imaged after a twofold application of the described procedure. The width of the clusters is 15 nm, as measured by STM.

The Mechanism

In order to understand the mechanism of the cluster formation on the substrate surface opposite to the STM tip, we consider the influence of the local variation of the Co^{2+} concentration during the anodic dissolution from the tip on the Nernst potential at the substrate surface in a model calculation. Since the thickness of the electrochemical double layer at the tip and the substrate surfaces is approximately 1 nm in a 0.5 M $NaSO_4$-1 mM Co^{2+} solution,[31] and hence much smaller than the typical tip substrate distance of 10-30 nm during the deposition procedure, the transfer of Co^{2+} from the tip to the substrate is determined by diffusion of Co^{2+}. Ion migration may be excluded, since the voltage drop at both substrate and STM tip essentially occurs across the electrochemical double layer. Thus the electric field in the remaining gap between tip and substrate may be assumed to be zero. Hence, the problem can be reduced to solving the diffusion equation[b] for Co^{2+} at appropriate boundary conditions, analogous to similar problems described in the literature.[32,33] The main contribution to the local variation of the Co^{2+} concentration at the substrate surface originates mainly from the STM tip apex, which is modeled as a hemisphere with a radius of $a = 50$ nm in agreement with a variety of SEM micrographs of different STM tips. During the short time of a few milliseconds of Co^{2+} emission from the STM tip (Fig. 3), this hemisphere represents a continuously Co^{2+} emitting surface source with a constant Co^{2+} emission rate. The emission rate is constant due to the constant Co^{2+} current during Co^{2+} emission from the STM tip, which is limited to approximately 520 nA by the current-voltage converter of our STM scanner, as shown by the current transient in Fig. 3.

[b] The diffusion equation in spherical coordinates is given by

$$\frac{\partial C}{\partial t} = \frac{1}{r^2}\left\{\frac{\partial}{\partial r}\left(Dr^2\frac{\partial C}{\partial r}\right) + \frac{1}{\sin\Theta}\frac{\partial}{\partial\Theta}\left(D\sin\Theta\frac{\partial C}{\partial\Theta}\right) + \frac{D}{\sin^2\Theta}\frac{\partial^2 C}{\partial\phi^2}\right\}$$

with the spherical coordinates r,Θ,ϕ, the ion concentration C, and the diffusion constant D.

Thus, the radial Co^{2+} concentration profile underneath the emitting STM tip is obtained by solving the diffusion equation for these particular boundary conditions. Integration of Co^{2+} emitting point sources across the hemisphere of the tip apex (Fig. 5) leads to the concentration profile $C(R,t_0)$ at distance $r = |\vec{R} - \vec{a}|$ from the STM tip apex surface (Fig. 5) at time $t = t_0$

$$C(R,t_0) = \frac{a j_{Co^{2+}}}{eR\sqrt{\pi D}} \times \int_0^{t_0} \frac{1}{\sqrt{t}}\left\{\exp\left(-\frac{(R-a)^2}{4Dt}\right) - \exp\left(-\frac{R^2+a^2}{4Dt}\right)\right\} dt$$

with $e = 1.602 \times 10^{-19}$ A s, the Co^{2+} diffusion constant $D = 7 \times 10^{-6}$ cm^2 s^{-1},[34] and the Co^{2+} emission current density $j_{Co^{2+}} = 520\,\text{nA} \times (S_{tip})^{-1}$, where S_{tip} denotes the total unisolated tip area. For the numerical calculations an unisolated tip area of $S_{tip} = 10\,\mu\text{m}^2$ was used. The influence of the substrate on the formation of the concentration profile underneath the STM tip has not been considered in this model calculation, but is addressed in the Discussion section.

Figure 6 shows the calculated time dependence of the Co^{2+} concentration at two distances $r = 5$ nm and $r = 40$ nm from the STM tip apex during Co^{2+} emission. A constant Co^{2+} concentration is

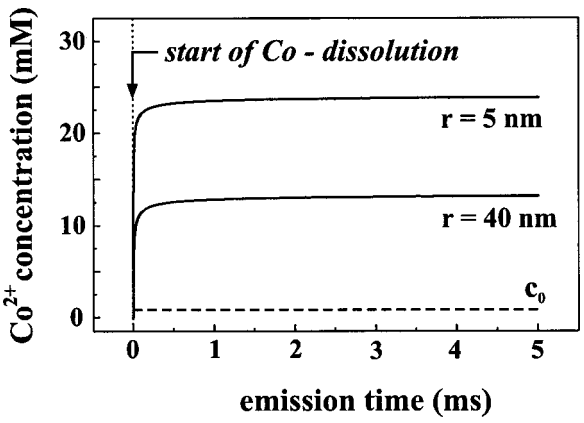

Figure 6. Calculated time dependence of the generation of the Co^{2+} concentration profile for different distances $r = 5$ nm and $r = 40$ nm from the STM tip surface for an emission time $t_0 = 5$ ms using Eq. 1. Co^{2+} emission current $I_{Co^{2+}} = 520$ nA, total uncovered tip area $S_{tip} = 10\,\mu\text{m}^2$. The concentration c_0 denotes the 1 mM Co^{2+} electrolyte concentration ($r = \infty$).

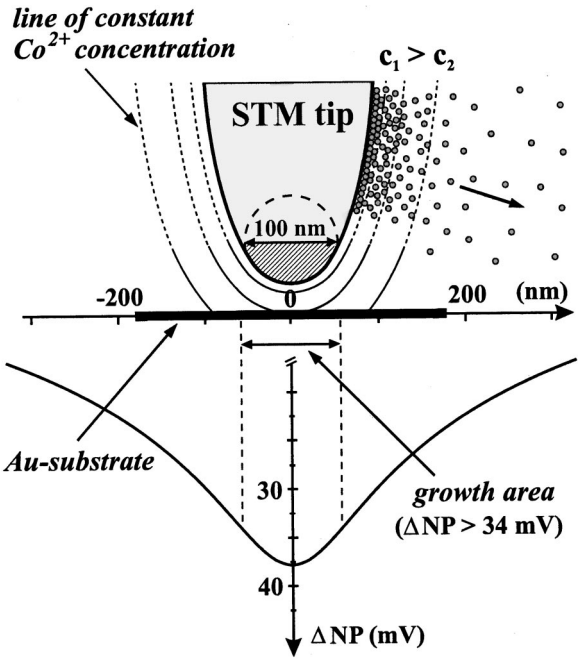

Figure 7. Calculated increase ΔNP of the Co^{2+}/Co Nernst potential at the substrate surface for a tip substrate distance $\Delta z = 20$ nm with respect to the Co^{2+}/Co Nernst potential of the 1 mM Co^{2+} solution. $I_{Co^{2+}} = 520$ nA, $S_{tip} = 10\,\mu m^2$. The solid lines of constant Co^{2+} concentration are calculated, the dashed lines of constant Co^{2+} concentration are extrapolated according to the STM tip shape. The diameter of the growth area is exemplarily shown assuming E_{WE} adjusted 34 mV below the maximum of the effective Nernst potential. (From Ref. 28.)

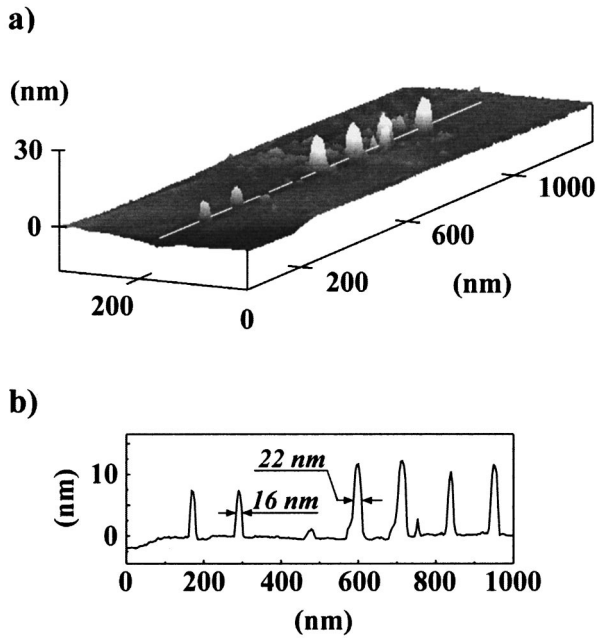

Figure 8. (a) STM image showing the dependence of the cluster height on the preadjusted cathodic charge Q_{cat}. First four deposition cycles: $Q_{cat} = 400$ pC; deposition cycle five to eight: $Q_{cat} = 600$ pC; $E_{WE} = -530$ mV, $\Delta z = 15$ nm. The third and the fourth cluster are missing. (b) Line profile along the white line.

reached within 100-200 μs, which means that the Co^{2+} diffusion profile around the STM tip can be considered stationary during the Co^{2+} emission time of 2-3 ms (Fig. 3b).

This stationary concentration profile results in a lateral variation of the Co^{2+} concentration at the substrate surface. According to the Nernst equation[c] this lateral variation of the Co^{2+} concentration is correlated with a lateral variation $\Delta NP(x,y)$ of the Co^{2+}/Co Nernst potential at the substrate surface, with respect to the Co^{2+}/Co Nernst potential of the 1 mM Co^{2+} electrolyte. Assuming a rotational symmetry about the axis of the STM tip, the lateral dependence of $\Delta NP(x,y)$ is considered in the following only in the x direction. Since the Co^{2+} emission from the STM tip results in an increase of the Co^{2+} concentration at the substrate surface, $\Delta NP(x)$ will be positive. The calculated increase of $\Delta NP(x)$ as a function of the lateral distance x from the center of the STM tip, with respect to the Nernst potential of an 1 mM Co^{2+} electrolyte, is shown in Fig. 7. Since $\Delta NP(x)$ adds to the uniform Nernst potential $E_{1\,mM}$ of the 1 mM Co^{2+} electrolyte, the diffusion profile results in a laterally varying effective Nernst potential $E_{eff}(x) = E_{1\,mM} + \Delta NP(x)$ underneath the STM tip with a maximum $E_{eff}^{max} = E_{1\,mM} + \Delta NP^{max}$ at $x = 0$ (Fig. 7).

Adjusting E_{WE} between the Nernst potential $E_{1\,mM}$ of the 1 mM Co^{2+} electrolyte and the maximum of this locally increased effective Nernst potential E_{eff}^{max}, the effective Nernst potential exceeds E_{WE} within a particular area underneath the STM tip (denoted as growth area in Fig. 7), and a localized deposition of Co is initiated.

[c] The Nernst potential E is given by the Nernst equation

$$E = E^0 + \frac{RT}{zF} \times \ln\left(\frac{a_{Co^{2+}}}{a_{Co}}\right)$$

with the standard potential E^0, $R = 8.314$ J K^{-1} mol^{-}, $T = 298$ K, $z = 2$, F = 96,480 A s, $a_{Co^{2+}} = f_{Co^{2+}} \times c_{Co^{2+}}$, the Co^{2+} activity coefficient $f_{Co^{2+}}$, and the Co^{2+} concentration $c_{Co^{2+}}$.

The Main Parameters

According to the presented model, the height and diameter of the deposited clusters is determined by (i) the radius a of the STM tip apex, (ii) the Co^{2+} emission current density $j_{Co^{2+}}$, (iii) the tip-substrate distance Δz, (iv) the predeposited tip charge Q_{cat}, and (v) the substrate potential E_{WE}. Thus, the two parameters height and diameter of the clusters are determined by at least five quantities, which are not independent of each other. Therefore, the STM tip diameter, $j_{Co^{2+}}$, and E_{WE} are held constant in the following, in order to study the influence of Q_{cat} and Δz on the shape of the deposited clusters in more detail.

Figure 8 shows a sequence of Co clusters grown by applying the described deposition sequence eight times. Between each sequence the lateral position of the STM tip was changed in linear direction. Whereas the first four sequences were applied with a predeposited cathodic tip charge of $Q_{cat} = 400$ pC, the sequences five to eight were applied with $Q_{cat} = 600$ pC. Since the Co deposition onto the tip can be controlled only by measuring the cathodic charge Q_{cat}, this charge was taken as measure for the predeposition of Co onto the STM tip, even if the anodic charges during Co dissolution from the STM tip are the important charges for the cluster formation. However, anodic and cathodic charges are proportional assuming a constant contribution of H_2 generation during Co^{2+} deposition onto the tip.[35] As is seen in the line profile of Fig. 8b, the height of the clusters scales with the amount of predeposited tip charge. The cluster height is 7.5 ± 0.5 nm in the case of $Q_{cat} = 400$ pC, and 11.5 ± 1 nm in the case of $Q_{cat} = 600$ pC. According to our model, the volume of the clusters should scale linearly with Q_{cat}, since the Co^{2+} emission time scales linearly with Q_{cat} due to the constant $j_{Co^{2+}}$ during Co^{2+} emission from the STM tip. However, nucleation of Co can occur only within the growth area on the substrate surface as illustrated in Fig. 7. The growth area depends only on the stationary Co^{2+} concentration profile, which is independent of the time of

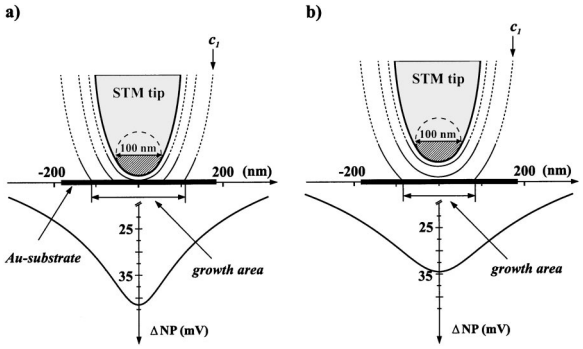

Figure 9. Model calculation of the dependence of the cluster diameter on the distance Δz between STM tip and substrate during the deposition procedure. The graphs show exemplarily two distances (a) $\Delta z = 5$ nm and (b) $\Delta z = 40$ nm. $I_{Co^{2+}} = 520$ nA, $S_{tip} = 10\,\mu m^2$. c_1 denotes the particular Co^{2+} concentration which results in an effective Nernst potential equal to E_{WE}. Nucleation is initiated within the growth area where the effective Nernst potential exceeds E_{WE}.

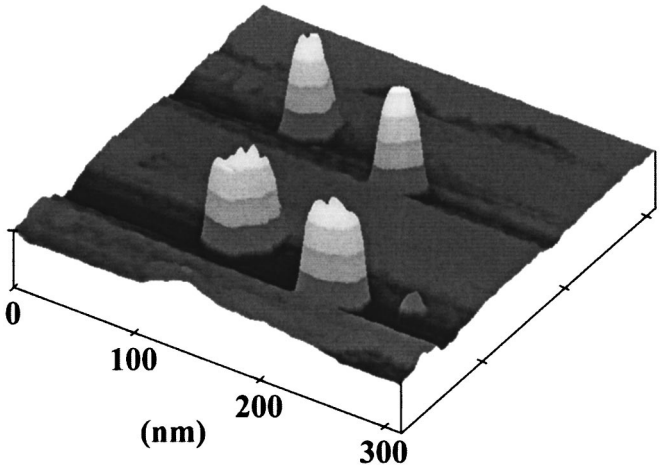

Figure 10. STM image showing the dependence of the cluster diameter on the distance Δz between STM tip and substrate during the deposition procedure. Upper row: $\Delta z = 15$ nm during deposition; lower row: $\Delta z = 10$ nm during deposition; $Q_{cat} = 800$ pC; $E_{WE} = -540$ mV. The fwhm of the clusters grown with $\Delta z = 15$ nm is 18 ± 1 nm, the fwhm of the clusters grown with $\Delta z = 10$ nm is 28 ± 1 nm, as measured by STM. Each gray scale value corresponds to a height of 1 nm. The lower baselines of the STM scans across the clusters, compared to the substrate surface, are a scan artifact.

Co^{2+} emission from the STM tip. Thus, Co growth occurs mainly in the z direction, but is confined laterally to within the growth area. This explains, that Q_{cat} scales linearly with the height of the clusters, and thus linearly with the cluster volume.

According to this explanation, the fwhm of the clusters should be independent of Q_{cat}. However, the STM measurement of Fig. 8 shows also an increase of the cluster fwhm with Q_{cat} from 16 nm at $Q_{cat} = 400$ pC to 22 nm at 600 pC. This increase of the cluster fwhm, unlike the correct height of the clusters, is due to an artifact of the STM measurement, caused by the convolution of the shape of the tip apex with the real cluster shape. The measured fwhm of clusters is enlarged, the higher the clusters are, even if the real cluster diameter remains constant. The absolute size of this effect depends in general on the actual tip shape and on the real cluster shape. However, the relative effect at objects of different height within a single STM image (i) can be determined if the STM tip remains unchanged during the measurement and (ii) is more or less independent of the actual tip apex diameter if the diameter is in the range of 20-100 nm. Assuming infinitely steep steps of height h and of height $1.5 \times h$, corresponding to our cluster heights of 7.5 and 11.5 nm (Fig. 8), the higher step results in an approximately 25% wider fwhm than the lower step. Thus, the observed broadening of the cluster fwhm in Fig. 8 of approximately 35% (from 16 nm at $Q_{cat} = 400$ pC to 22 nm at $Q_{cat} = 600$ pC in Fig. 8) is mainly caused by this artifact. The fwhm of the clusters turns out to be independent of Q_{cat} in good agreement with our model presented above.

As can be seen from Fig. 7, a decrease of Δz results in an increase of the Co^{2+} concentration at a fixed lateral position of the substrate surface, and thus, according to the Nernst equation, in an increase of the effective Nernst potential at this particular position. Therefore, the diameter of the growth area is also expected to increase according to our model. This is shown explicitly for two tip-substrate distances $\Delta z = 5$ nm and 40 nm in Fig. 9. It seems quite surprising that the growth area and hence the cluster diameter should decrease with increasing tip-substrate distance, and vice versa. However, the experimental finding in Fig. 10 proves this prediction. The only parameter which was varied between the deposition of the upper and lower row of clusters was the tip-substrate distance Δz. Whereas the measured fwhm of the clusters deposited at $\Delta z = 15$ nm is 18 ± 1 nm (Fig. 10, upper row), the fwhm of the clusters deposited at $\Delta z = 10$ nm is 28 ± 1 nm (Fig. 10, lower row). Remarkably, all clusters are approximately equal in height due to the constant Q_{cat} during each of the four deposition cycles. Unlike the situation in Fig. 8, the convolution of the tip apex shape with the real cluster shape would not significantly change the ratio of the cluster fwhms, since all clusters in Fig. 10 are equal in height. Thus, the measured decrease of the cluster fwhm from 28 to 18 nm upon increase of Δz from 10 to 15 nm may be assumed to be correct. The volume of the clusters decreases with increasing Δz if Q_{cat} is held constant.

Discussion

The localized electrodeposition on the nanometer scale using the tip of a STM as nanoelectrode allows the electrochemical growth of quasi zero-dimensional (metal) clusters. Even if the three-dimensional delocalized nucleation of metal clusters has been widely studied for more than 20 years,[36] the active deposition of single clusters on a surface opens up the exciting possibility to investigate the properties of individual clusters. Since the nanoelectrode is made from electrochemically inert Au, and not from, *e.g.*, Co, the technique allows the electrodeposited clusters to be studied simultaneously by *in situ* STM. The substrate/deposit system $Au(111)/Co^{2+}$ shows no underpotential deposition within the measurement accuracy of cyclic voltammetry. Therefore, it is a good example for the universality of the technique. The results may be representative also for other substrate/deposit systems, in particular for underpotential deposition systems. This has been proven by the deposition of Cu clusters on Au surfaces.[37]

The experimentally observed dependencies of the cluster diameter on the distance Δz between the STM tip and substrate during deposition (Fig. 10), the dependence of the cluster height on the cathodic charge Q_{cat} predeposited onto the STM tip (Fig. 8), as well as the independence of the cluster diameter on Q_{cat} confirm the predictions of our Co^{2+} diffusion model.

The dependence of the cluster size on the STM tip apex diameter and the dependence on the Co^{2+} current density $j_{Co^{2+}}$ during Co^{2+} emission from the STM tip are difficult to study *in situ*. An increase of the Co^{2+} current density is expected to result in an increase of the lateral variation ΔNP of the Co^{2+}/Co Nernst potential at the substrate surface underneath the STM tip. This was optimized in our experiments by changing the current-voltage conversion gain of our current-voltage converter to allow up to 520 nA tip current. A further increase of $j_{Co^{2+}}$ can be achieved either by increasing the Co^{2+}

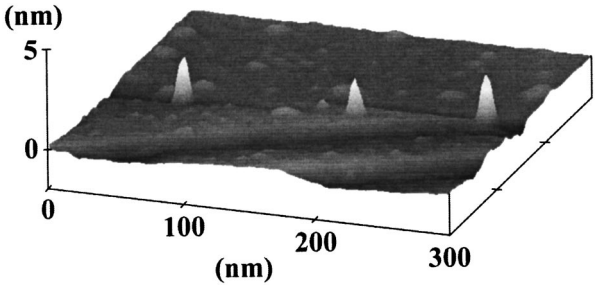

Figure 11. STM image showing three Co clusters on Au(111) after deposition with $\Delta z = 10$ nm and $Q_{cat} = 400$ pC; $E_{WE} = -535$ mV. The height of the clusters is 2.5 ± 0.5 nm, the fwhm is 9.5 ± 0.5 nm, as measured by STM.

emission current or by decreasing the unisolated tip surface area, which was approximately 10 μm^2 in our experiments. A positive consequence of a further increase of $j_{Co^{2+}}$ would be a less critical adjustment of the substrate potential E_{WE} which had to be adjusted within approximately 40 mV $= \Delta NP^{max}$ at our experimental conditions. A rough estimate using Eq. 1 shows that an uncovered tip area of only 1 μm^2 would result in a maximum increase of the effective Nernst potential by about $\Delta NP^{max} \approx 70$ mV. Hence, this range would be available for adjustment of the substrate potential.

Nevertheless, the available potential range ΔNP^{max} between the Nernst potential of the 1 mM Co^{2+} electrolyte solution and the maximum of the effective Nernst potential at the substrate surface underneath the STM tip is large enough to adjust E_{WE} well above the equilibrium potential for delocalized nucleation on the substrate.

According to our model, the diameter of the nucleation area on the substrate becomes smaller, if the substrate potential E_{WE} is adjusted to be more positive, because the Co^{2+}/Co Nernst potential is exceeded only within a smaller substrate area. Thus, the cluster diameter could be varied by changing E_{WE} by a few millivolts.

It seems to be important that the parameters Δz, Q_{cat}, and E_{WE} can be adjusted independently, thus allowing a nearly independent adjustment of cluster diameter and cluster height. This feature is remarkable, because it allows for tailoring lateral extension and aspect ratio of the structures independently, as may be required for specific applications.

The conical shape of the clusters as seen in the STM images becomes more pronounced with decreasing cluster diameter, as seen from comparison of, *e.g.*, Fig. 10 and 11. This is an artifact of the STM measurement, representing the convolution of the real cluster shape with the shape of the STM tip apex. It becomes increasingly important when studying structures both of lateral sizes in the lower nanometer range, and simultaneously of high aspect ratio.

According to our model, the cluster diameter decreases both with increasing distance between STM tip and substrate and with increasing E_{WE}. These dependencies could compensate large tip diameters, and thus result in the observed small structure sizes. Despite the diameter of our STM tips being approximately 100 nm, clusters with diameters below 10 nm, as measured by STM, could be grown (Fig. 11). Additionally, small cluster sizes could be achieved by exploiting nucleation overpotentials, which result in a larger ΔNP necessary for nucleation, and hence a smaller nucleation area on the substrate. Such overpotentials are likely present in our system as seen from the cyclic voltammogram (Fig. 2).

The absolute value of E_{tip} during loading and emission of Co, as shown in Fig. 2 and 3, are not critical for the diameter of the nucleation area on the substrate, since this area is determined only by the Co^{2+} concentration profile around the STM tip, independent of the particular tip potential. The only essential assumption for the presented model is a constant Co^{2+} emission rate from the STM tip. Qualitatively, the results would remain the same, even if the Co^{2+} emission rate from the STM tip would not be constant; however, the exact solution of the diffusion equation would be much more complicated than in the presented case.

The influence of the substrate surface on the Co^{2+} diffusion profile has not been taken into account in our model calculation. It is obvious, that the substrate prevents a further Co^{2+} diffusion into the volume of the substrate, which would take place in the case of a missing substrate. Hence, the presence of the substrate should result in an additional increase of Co^{2+} concentration in the gap between tip and substrate, thus resulting in an amplification of the effect. Immediately after initiation of the Co^{2+} nucleation, the growth area on the substrate can be assumed to be a Co^{2+} sink, which reduces the back diffusion of Co^{2+} into the gap between substrate surface and STM tip. This effect would result in a slightly decreasing Co^{2+} concentration in front of the growth area, and thus in a slightly decreasing ΔNP. In order to maintain the Co^{2+} deposition, the initial enhancement of the Co^{2+} concentration, and hence of the initial ΔNP, must be large enough to compensate for this effect.

This kind of localized electrochemical deposition is not restricted to STM, but can also be applied in the electrochemical atomic force microscope (AFM). The only requirement is a conductive probe in order to use the probe as an electrochemical nanoelectrode. A simultaneous lateral translation of the tip during Co^{2+} emission from the tip may be applied to grow continuous lines instead of single clusters. This would open the possibility for fabricating well-defined nanoscale objects in view of nanotechnological applications. In this context, it is important to note, that the repetition rate of the cluster deposition may be at least as high as 10 Hz (Fig. 3), which would allow one to grow more complicated structures on reasonable time scales.

Summary

The electrochemical deposition of Co clusters, using a STM tip as an electrochemical nanoelectrode poised at a distance of typically 20 nm from the substrate surface, can be described assuming Co transfer from the STM tip to the substrate by diffusion. The influence of the main parameters on the diameter and height of the deposited clusters can be well understood. The scanning probe-based electrochemical deposition, as presented in this paper, allows the active formation of structures at precisely predefined locations on the substrate surface, even in a system showing a relatively weak substrate/deposit interaction compared to the strong interaction of underpotential deposition systems. Therefore, the results seem to be of importance in view of the current variety of reported approaches of scanning probe based nanostructuring techniques. Our results may help to distinguish among different mechanisms which are likely involved in the procedures reported so far in the literature.

Acknowledgments

The authors are indebted to H. Menge for supporting us with high quality Au(111) crystals. Financial support by the Deutsche Forschungsgemeinschaft under contract KI 358/1-2 and SCHI492/1-2 is gratefully acknowledged.

Max-Planck-Institut für Mikrostrukturphysik assisted in meeting the publication costs of this article.

References

1. D. Awschalom and D. P. DiVincenzo, *Phys. Today*, **1995**, 43 (April).
2. P. D. Ye, D. Weiss, R. R. Gerhardts, M. Seeger, K. von Klitzing, K. Eberl, and H. Nickel, *Phys. Rev. Lett.*, **74**, 3013 (1995).
3. M. Löhndorf, A. Wadas, G. Lütjering, D. Weiss, and R. Wiesendanger, *Z. Phys. B: Condens. Matter* **101**, 1 (1996).
4. S. Mancini, A. M. Martins, and P. Tombesi, *Phys. Rev. A*, **61**, 12303 (1999).
5. K. Matsumoto, M. Ishii, K. Segawa, Y. Oka, B. J. Vartanian, and J.S. Harris, *Appl. Phys. Lett.*, **68**, 34 (1996).
6. K. Matsumoto, Y. Gotoh, T. Maeda, J. A. Dagata, and J. S. Harris, *Appl. Phys. Lett.*, **76**, 239 (2000).
7. S. Y. Chou, M. Wei, P. R. Kraus, and P. B. Fischer, *J. Vac. Sci. Technol. B*, **12**, 3695 (1994).

8. J. Shen, R. Skomski, M. Klaua, H. Jenniches, S. Sundar Manoharan, and J. Kirschner, *Phys. Rev. B*, **56**, 2340 (1997).
9. O. Fruchard, M. Klaua, J. Barthel, and J. Kirschner, *Phys. Rev. Lett.*, **83**, 2769 (1999).
10. D. P. DiVincenzo and D. Loss, *J. Magn. Magn. Mater.*, **200**, 202 (1999).
11. M. Watanabe, H. Sei, and P. Stonehart, *J. Electroanal. Chem.*, **261**, 375 (1989).
12. T. Frelink, W. Visscher, and J. A. R. van Veen, *J. Electroanal. Chem.*, **382**, 65 (1995).
13. M. Haruta, *Catal. Today*, **36**, 153 (1997).
14. G. Staikov, W. J. Lorenz, and E. Budevski, in *Imaging of Surfaces and Interfaces*, J. Lipkowski and P. N. Ross, Editors, p. 1, Wiley-VCH, Weinheim (1999).
15. W. Li, J. A. Virtanen, and R. M. Penner, *Appl. Phys. Lett.*, **60**, 1181 (1992).
16. W. Li, J. A. Virtanen, and R. M. Penner, *J. Phys. Chem.*, **96**, 6529 (1996).
17. W. Li, G. S. Hsiao, D. Harris, R. M. Nyffenegger, J. A. Virtanen, and R. M. Penner, *J. Phys. Chem.*, **100**, 20103 (1996).
18. R. Schuster, V. Kirchner, X. H. Xia, A. M. Bittner, and G. Ertl, *Phys. Rev. Lett.*, **80**, 5599 (1998).
19. S. Wirth, M. Field, D. D. Awschalom, and S. von Molnar, *Phys. Rev. B*, **57**, R14028 (1998).
20. S. Wirth, S. von Molnar, M. Field, and D. D. Awschalom, *J. Appl. Phys.*, **85**, 5249 (1999).
21. R. T. Pötzschke, A. Fröse, W. Wiesbeck, G. Staikov, and W. J. Lorenz, in *Proceedings of the Third Symposium on Electrochemically Deposited Thin Films*, M. Paunovich and D. A. Scherson, Editors, Vol. 96-19, p. 21, The Electrochemical Society Proceeding Series, Pennington, NJ (1997).
22. R. T. Pötzschke, G. Staikov, W. J. Lorenz, and W. Wiesbeck, *J. Electrochem. Soc.*, **146**, 141 (1999).
23. R. Ullmann, T. Will, and D. M. Kolb, *Chem. Phys. Lett.*, **209**, 238 (1993).
24. R. Ullmann, T. Will, and D. M. Kolb, *Ber. Bunsenges. Phys. Chem.*, **99**, 1414 (1995).
25. D. M. Kolb, R. Ullmann, and T. Will, *Science*, **275**, 1097 (1997).
26. D. M. Kolb, R. Ullmann, and J. C. Ziegler, *Electrochim. Acta*, **43**, 2751 (1998).
27. D. Hofmann, W. Schindler, and J. Kirschner, *Appl. Phys. Lett.*, **73**, 3279 (1998).
28. W. Schindler, D. Hofmann, and J. Kirschner, *J. Appl. Phys.*, **87**, 7007 (2000).
29. S. Meltzer and D. Mandler, *J. Electrochem. Soc.*, **142**, L82 (1995).
30. F. Forouzan and A. J. Bard, *J. Phys. Chem. B*, **1997**, 10876.
31. C. H. Hamann and W. Vielstich, *Elektrochemie I*, VCH, Weinheim (1985).
32. H. Carslaw and J. C. Jaeger, *Conduction of Heat in Solids*, Oxford University Press, Oxford (1959).
33. J. Crank, *The Mathematics of Diffusion*, Oxford University Press, Oxford (1967).
34. P. Vaný́sek, in *CRC Handbook of Chemistry and Physics*, D. R. Lide and H. P. R. Frederikse, Editors, pp. 5-90, CRC Press, Boca Raton, FL (1993).
35. W. Schindler, Th. Koop, and J. Kirschner, *Z. Phys. Chem. (Munich)*, **208**, 93 (1999).
36. E. Budevski, G. Staikov, and W. J. Lorenz, *Electrochemical Phase Formation and Growth*, Wiley-VCH, Weinheim (1996).
37. G. Staikov, W. J. Lorenz, and E. Budevski, in *Imaging of Surfaces and Interfaces*, J. Lipkowski and P. N. Ross, Editors, p. 52, Wiley-VCH, Weinheim (1999).